A PARAMETRIC BAYESIAN RMC GAMMA-RAY IMAGE RECONSTRUCTION

Branko Ristic and Michael D. Roberts

DSTO
Land Division
Melbourne, Australia

ABSTRACT

Rotational modulation collimation (RMC) is a technique commonly used for standoff imaging of radiological sources in the context of homeland security. The paper presents a novel method for gamma ray image reconstruction from modulation signals acquired by a RMC detector prototyped by DSTO. The image is represented in a parametric form as a weighted sum of Gaussian radial basis functions. The problem is thus formulated as a parameter estimation problem and solved in the Bayesian framework using a multi-stage Monte Carlo technique known as progressive correction. A comparison with EM and MAP image reconstruction algorithms is provided.

***Index Terms*—** Image reconstruction, emission tomography, homeland security, Bayesian Monte Carlo estimation

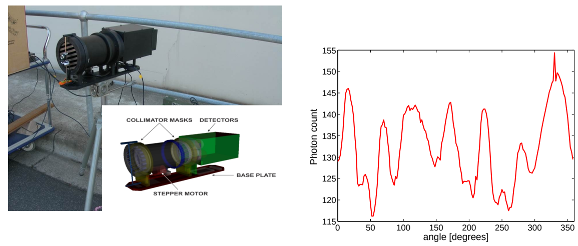

(a) (b)

Fig. 1. (a) A picture of the RMC gamma imaging prototype; (b) an example of a modulated detector response for a far-field point source of gamma radiation

1. INTRODUCTION

The potential for misuse of radiological materials, either deliberate or accidental, has been well recognized [1]. DSTO has recently built a prototype of a standoff imaging gamma radiation detector which can be used to determine the exact location of a radiological source within its field of view [2]. The prototype is based on the technique known as rotational modulation collimation (RMC), previously used in astronomy, medical imaging and homeland security [3]. The RMC technique uses two attenuating masks, separated by a known distance, co-rotating on a cylinder in front of one or more gamma ray detectors (see Fig.1.a). As the masks rotate, the bars obscure the radiation sources from the gamma detectors, by an amount that varies as a function of the mask rotation angle. Consequently, the count of photons coming from the radioactive sources within the field-of-view (FoV) of the device are modulated, producing thus a "fingerprint" that encodes the information about the location of each source. Fig.1.b illustrates a modulated detector response, created by a far field point source, placed within the FoV. The abscissa on the graph in Fig.1.b is the rotation angle, while the ordinate is the photon count.

The goal of the standoff gamma imaging device is to reconstruct an image in which the pixel brightness corresponds to the gamma radiation source intensity. The input for an image reconstruction algorithm is the measured modulated detector response, such as the one in Fig.1, affected by Poisson fluctuations. Since the typical number of image pixels N is much greater than the number of measurements M collected by the RMC device (for example, the DSTO prototype features $N = 10816$ pixels and $M = 540$ measured modulations), image reconstruction in this context is a very difficult ill-posed problem.

Formally, the image reconstruction problem using an RMC gamma detector can be cast in the same mathematical framework as emission tomography reconstruction, developed and studied extensively for the purpose of medical imaging [4]. The most popular algorithm in this context is the iterative expectation-maximization (EM) image reconstruction algorithm [5]; consequently it has been implemented in RMC prototypes [3] and [2]. The EM algorithm, however, is known to suffer from the grainy, speckled appearance of medical images. When applied to RMC gamma image reconstruction, the EM algorithm performs well only for point sources; for extended, plume-like sources, it produces multiple bright speckles.

A solution to EM generated speckled medical images was to incorporate smoothness in the reconstruction process. This has been achieved in a principled manner using the Bayesian estimation framework, with the Gibbs prior distribution imposed to regularize the solution [6]. The result is the maximum a posteriori (MAP) image reconstruction, which is the current state-of-the art in emission tomography reconstruction for medical imaging. Recent research is primarily focused on the design of the Gibbs prior [7], [8].

There are, however, important differences between emission tomography reconstruction for medical imaging and the image reconstruction problem using an RMC detector in the context of homeland security. On one hand, the measurements collected by an RMC detector are less informative ($N \gg M$), making the task more difficult. On the other hand, the expected number of radiological sources in the FoV is typically very small (maximum two or three) and their shape can be approximated with reasonable accuracy by a simple parametric model (e.g. an ellipse or a circle). In addition, image reconstruction for homeland security does not need to be as detailed as in medical imaging applications. This motivates the approach proposed in this paper: a parametric Bayesian radiological source image reconstruction for an RMC gamma detector. An image is represented by a weighted sum of Gaussian functions (radial or ellipsoidal). Instead of attempting to estimate the brightness in all N pixels of the gamma radiation image, the proposed parametric approach aims to estimate a relatively small number of shape parameters (e.g. for a circle, four parameters per source) for each radiological source. The parameter estimation problem is solved in the Bayesian framework using a multi-stage Monte Carlo technique known as the progressive correction (PC) [9].

The paper is organised as follows. The mathematical formulation of the problem is stated in Sec.2. The proposed algorithm is described in Sec.3. Numerical results are presented in Sec.4. Finally, the concluding remarks including a discussion of future work are given in Sec.5.

2. PROBLEM SPECIFICATION

The image consists of $N = L \times L$ pixels. The RMC gamma detector measurement (modulated detector response, similar to the one shown in Fig.1) can be modelled as:

$$y_i \sim \mathcal{P}_{y_i}(h_i), \qquad (i = 1, \ldots, M) \tag{1}$$

where $y_i \in \mathbb{N}_0$ (a non-negative integer) is the number of photons counted in the rotation i of the RMC detector, and $\mathcal{P}_n(\nu) = \nu^n \exp(-\nu)/n!$ is the Poisson distribution. The Poisson mean count h_i in (1) is modelled as

$$h_i = \sum_{j=1}^{N} A_{ij}\lambda_j \tag{2}$$

where λ_j is the activity of the jth pixel and $\mathbf{A} = \{A_{ij}\}$ is the system matrix, which can be determined from the design of the rotating masks in the instrument (therefore $\mathbf{A}$ is assumed known). The goal is to reconstruct the image, that is the vector $\boldsymbol{\lambda} = [\lambda_1, \ldots, \lambda_N]^\intercal$, from the count measurement vector $\mathbf{y} = [y_1, \ldots, y_M]^\intercal$.

While the common strategies for image reconstruction solve for the image vector $\boldsymbol{\lambda}$ in a non-parametric form, we represent the image by the weighted sum of Q Gaussian radial basis functions [10]. The activity (brightness) in pixel $j = 1, \ldots, N$ is then modelled as:

$$\lambda_j(\boldsymbol{\theta}) = \sum_{k=1}^{Q} \lambda_{jk}(\boldsymbol{\theta}) \tag{3}$$

where

$$\lambda_{jk}(\boldsymbol{\theta}) = w_k \exp\Big\{ -\frac{(x_j - \bar{x}_k)^2 + (y_j - \bar{y}_k)^2}{\sigma_k^2} \Big\} \tag{4}$$

is the activity in pixel j due to the Gaussian component k. The explanation of terms in (4) is as follows; $w_k \geq 0$ is the weight assigned to the kth Gaussian component; (x_j, y_j) denotes the coordinates of the jth pixel; $(\bar{x}_k, \bar{y}_k)$ and $\sigma_k > 0$ are the mean and the standard deviation, respectively, of the kth Gaussian radial basis function.

The image reconstruction problem amounts to estimating the $4Q$-dimensional parameter vector $\boldsymbol{\theta} = [\mathbf{w}^\intercal \; \bar{\mathbf{x}}^\intercal \; \bar{\mathbf{y}}^\intercal \; \boldsymbol{\sigma}^\intercal]^\intercal$, where $\mathbf{w} = [w_1, \cdots, w_Q]^\intercal$, $\bar{\mathbf{x}} = [\bar{x}_1, \ldots, \bar{x}_Q]^\intercal$, $\bar{\mathbf{y}} = [\bar{y}_1, \ldots, \bar{y}_Q]^\intercal$ and $\boldsymbol{\sigma} = [\sigma_1, \ldots, \sigma_Q]^\intercal$. This completes the specification of the measurement function $h_i(\boldsymbol{\theta})$ of the ith "sensor" (rotational angle), see (2), as a function of the parameter vector $\boldsymbol{\theta}$. In the matrix form, $\mathbf{h}(\boldsymbol{\theta}) = \mathbf{A}\,\boldsymbol{\lambda}(\boldsymbol{\theta})$, with $\mathbf{h}(\boldsymbol{\theta}) = [h_1(\boldsymbol{\theta}), \ldots, h_M(\boldsymbol{\theta})]^\intercal$.

The problem can be now specified as follows. Given a prior probability density function (PDF) over the parameter space, $\pi_0(\boldsymbol{\theta})$, and the count measurement vector $\mathbf{y} = [y_1, \ldots, y_M]^\intercal$, the problem is to estimate the posterior density

$$\pi(\boldsymbol{\theta}|\mathbf{y}) \propto p(\mathbf{y}|\boldsymbol{\theta})\,\pi_0(\boldsymbol{\theta}) \tag{5}$$

where $p(\mathbf{y}|\boldsymbol{\theta})$ is the likelihood function. Making an assumption that count measurements at different rotational angles are mutually independent (only approximately true, because some correlation between neighbouring angles exists), the likelihood function can be written as:

$$p(\mathbf{y}|\boldsymbol{\theta}) = \prod_{i=1}^{M} \frac{h_i(\boldsymbol{\theta})^{y_i}}{y_i!} \exp\{-h_i(\boldsymbol{\theta})\} \tag{6}$$

3. ESTIMATION OF THE POSTERIOR PDF

Computation of the posterior density (5) is a nontrivial task and usually involves numerical approximations. The difficulty is that the prior density is almost always considerably more diffuse than the likelihood. Progressive correction [9] is a Bayesian technique which computes the posterior density in stages. The initial stage starts with the prior, while each following stage is progressively closer to the posterior PDF. The intermediate posterior at stage $t = 1, 2, \ldots, T$ is given by:

$$\begin{aligned} \pi_t(\boldsymbol{\theta}|\mathbf{y}) &\propto p(\mathbf{y}|\boldsymbol{\theta})^{\Gamma_t}\pi_0(\boldsymbol{\theta}) \\ &\propto p(\mathbf{y}|\boldsymbol{\theta})^{\gamma_t}\pi_{t-1}(\boldsymbol{\theta}|\mathbf{y}) \end{aligned} \tag{7}$$

where $\Gamma_t = \sum_{j=1}^{t}\gamma_j$ with $\gamma_j \in (0, 1]$ and $\Gamma_T = 1$. In this way Γ_t is a monotonically increasing function of t, with an upper bound of one. Note that the intermediate posterior PDF (for $1 \leq t < T$) is a broader (flattened) version of the true posterior. It indeed progressively becomes closer to the posterior PDF, so that at the final stage $t = T$, when $\Gamma_T = 1$ we have $\pi_T(\boldsymbol{\theta}|\mathbf{y}) \equiv \pi(\boldsymbol{\theta}|\mathbf{y})$.

Progressive correction can be implemented using the Monte Carlo importance sampling method. This involves drawing samples from an importance density and assigning weights to them. Suppose at the $(t-1)$th stage of the PC (where $t \geq 1$), a Monte Carlo representation of the intermediate posterior PDF $\pi_{t-1}(\boldsymbol{\theta})$ is available and consist of S sample-weight pairs: $\{\boldsymbol{\theta}_{t-1}^{(s)}, w_{t-1}^{(s)}\}_{1\leq s\leq S}$. At the initial stage, this representation is formed by drawing samples $\boldsymbol{\theta}_0^{(s)} \sim \pi_0$, and setting the weights $w_0^{(s)} = 1/S$. The approximation of $\pi_{t-1}(\boldsymbol{\theta})$ can be written as

$$\widehat{\pi}_{t-1}(\boldsymbol{\theta}) = \sum_{s=1}^{S} w_{t-1}^{(s)}\,\delta_{\boldsymbol{\theta}_{t-1}^{(s)}}(\boldsymbol{\theta}). \tag{8}$$

where $\delta_{\mathbf{y}}(\mathbf{x})$ is the standard Dirac delta concentrated at $\mathbf{y}$. In order to obtain the set of sample-weight pairs at the next stage t, that is $\{\boldsymbol{\theta}_t^{(s)}, w_t^{(s)}\}_{1\leq s\leq S}$, first we update the importance weights according to (7):

$$\tilde{w}_t^{(s)} = \beta p(\mathbf{y}|\boldsymbol{\theta}_{t-1}^{(s)})^{\gamma_t}\, w_{t-1}^{(s)} \tag{9}$$

where β is a normalising constant (the weights sum to one). Importance weights $\{\tilde{w}_t^{(s)}\}_{1\leq s\leq S}$ are assigned to samples $\{\boldsymbol{\theta}_{t-1}^{(s)}\}_{1\leq s\leq S}$. In order to derive any benefits from PC, it is necessary to remove the lower weighted members of the sample $\{\boldsymbol{\theta}_{t-1}^{(s)}\}_{1\leq s\leq S}$ and diversify the remaining ones. Hence the next step is resampling, followed by the Metropolis-Hastings step.

Resampling involves selecting S indices $i_1, i_2, \ldots, i_S$ from $\{1, \ldots, S\}$, such that the probability of selecting index i_s equals the weight $\tilde{w}_t^{(s)}$. The samples at stage t are then formed using the Metropolis-Hastings algorithm for $s = 1, \ldots, S$, i.e.

$$\boldsymbol{\theta}_t^{(s)} = \begin{cases} \boldsymbol{\theta}_{t-1}^{(i_s,*)}, & \text{if } u < \alpha \\ \boldsymbol{\theta}_{t-1}^{(i_s)}, & \text{otherwise} \end{cases}, \tag{10}$$

where $u \sim \mathcal{U}_{[0,1]}$ and α is the acceptance probability

$$\alpha = \min\left\{1, \frac{p(\mathbf{y}|\boldsymbol{\theta}_{t-1}^{(i_s,*)})\pi_0(\boldsymbol{\theta}_{t-1}^{(i_s,*)})}{p(\mathbf{y}|\boldsymbol{\theta}_{t-1}^{(i_s)})\pi_0(\boldsymbol{\theta}_{t-1}^{(i_s)})}\right\}. \tag{11}$$

Diversification of samples is achieved by proposing samples $\boldsymbol{\theta}_{t-1}^{(i_s,*)} = \boldsymbol{\theta}_{t-1}^{(i_s)} + \epsilon_s$, where ϵ_s is drawn from the Gaussian kernel density whose covariance matrix equals the sample covariance of $\{\boldsymbol{\theta}_{t-1}^{(s)}\}_{1\leq s\leq S}$. Note that due to resampling, the weights assigned to $\{\boldsymbol{\theta}_t^{(s)}\}_{1\leq s\leq S}$ are uniform, i.e. $w_t^{(s)} = 1/S$, $s = 1,\ldots,S$. The basic steps of this technique are summarised in Algorithm 1. Since the weights are uniform, they feature only in lines 5 and 6, where they are used in resampling.

Algorithm 1 : Progressive correction

1: **Input**: $\mathbf{y}, S$
2: Select correction factors $\gamma_1,\ldots,\gamma_T$.
3: Draw $\boldsymbol{\theta}_0^{(s)} \sim \pi_0$, for $s = 1,\ldots,S$
4: **for** $t = 1,\ldots,T$ **do**
5: Comp: $\tilde{w}_t^{(s)} = \beta'[p(\mathbf{y}|\boldsymbol{\theta}_{t-1}^{(s)})]^{\gamma_t}$, for $s = 1,\ldots,S$
6: Resample: draw $\{i_s\}_{1\leq s\leq S}$ based on $\{\tilde{w}_t^{(s)}\}_{1\leq s\leq S}$
7: **for** $s = 1,\ldots,S$ **do**
8: Propose $\boldsymbol{\theta}_t^{(s,*)} = \boldsymbol{\theta}_{t-1}^{(i_s)} + \epsilon_s$
9: Compute α according to (11)
10: Draw $u \sim \mathcal{U}_{[0,1]}$
11: Adopt $\boldsymbol{\theta}_t^{(s)}$ based on (10)
12: **end for**
13: **end for**
14: **Output**: $\{\boldsymbol{\theta}_T^{(s)}\}_{1\leq s\leq S}$

For $Q > 1$, the proposed algorithm is affected by the "permutation invariance" [11]: a sample $\boldsymbol{\theta}_t^{(s)}$ is equivalent to any of the $Q!$ permutations of its components. This ambiguity can be resolved sooner (typically after $T/2$ stages), by finding the sample with the highest importance weight, and then by imposing its permutation to all other samples (by rearranging appropriately the order of their components).

4. NUMERICAL RESULTS

4.1. Real data, point source

First we demonstrate the algorithm using a real dataset collected using the DSTO RMC prototype, with a single point source (Cs-137) placed at the distance of 260m. The prior PDF is adopted as $\pi(\boldsymbol{\theta}) = \pi_0(w)\pi_0(\bar{x})\pi_0(\bar{y})\pi_0(\sigma)$, where

$$\pi_0(w) = \mathcal{G}(w;1,2), \qquad \pi_0(\bar{x}) = \mathcal{U}_{[0.5,104.5]}(\bar{x}),$$
$$\pi_0(\bar{y}) = \mathcal{U}_{[0.5,104.5]}(\bar{y}), \qquad \pi_0(\sigma) = \mathcal{G}(\sigma;1.2,1) \tag{12}$$

Here $\mathcal{G}(\cdot;\kappa,\rho)$ is the Gamma PDF with shape parameter κ and scale parameter ρ. The progressive correction was implemented with $T = 40$ stages, using correction factors that satisfy $\gamma_{t+1}/\gamma_t = 1.2$, for $t = 1,\ldots,T-1$. The sample size was set to $S = 4000$ and $Q = 1$. Fig. 2 shows the field of view with the cloud of samples (yellow coloured dots) indicating the location of the source (coinciding with the true location). The source location samples were converted appropriately from the gamma image pixel coordinates to the video image. Fig. 2 also illustrates the prior PDF (red line) and the posterior PDF (blue line) for the weight w and standard deviation σ.

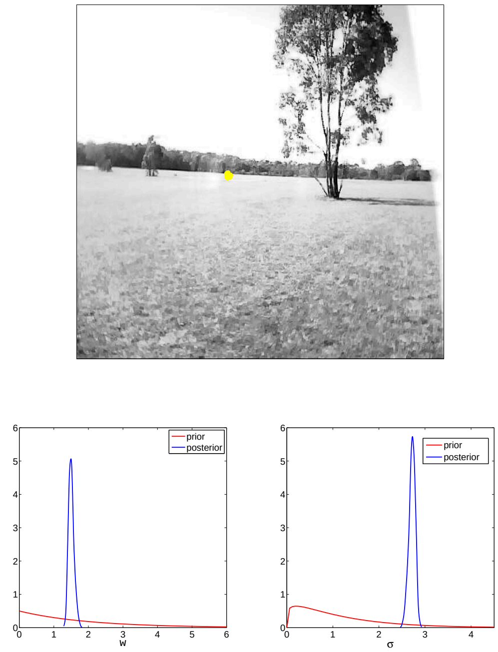

Fig. 2. Results using real data and a point source (Cs-137)

We point out that image reconstruction using the EM algorithm in this scenario provides satisfactory results. Next we consider extended sources. Real data with extended sources are currently unavailable, hence the numerical study is carried out via simulations.

4.2. Simulations, extended sources

Fig. 3 shows the single-run results for the case of one (left column) and two (right column) extended sources. The original images are in the first row, followed by images reconstructed using the proposed parametric Bayesian (PC, Algorithm 1), EM and the MAP image reconstruction method. The PC was implemented with $T = 20$ stages; its correction factors satisfy $\gamma_{t+1}/\gamma_t = 1.2$; the number of samples was $S = 6000$ and $Q = 2$. The prior PDFs were the same as in (12). The shown EM and MAP reconstructed images were obtained after 250 iterations. The Gibbs prior was used with the neighborhood window size of 11×11 pixels.

Fig. 3 demonstrates the superior performance of the proposed method, in comparison with EM and MAP image reconstruction algorithms.

Quantitative error performance of the three considered image reconstruction algorithms (EM, MAP and the proposed) was obtained by averaging over 100 Monte Carlo runs, with the error $\mathcal{E}$ between the original image $\boldsymbol{\lambda}$ and the estimated $\widehat{\boldsymbol{\lambda}}$, defined as:

$$\mathcal{E} = \sum_{j=1}^{N} |\lambda_j - \widehat{\lambda}_j|.$$

The proposed parametric algorithm creates an image estimate $\widehat{\boldsymbol{\lambda}}$ by first computing the MAP estimate $\widehat{\boldsymbol{\theta}}$ from the sample $\{\boldsymbol{\theta}_T^{(s)}\}_{1 \le s \le S}$ produced by Algorithm 1, followed by application of (3) and (4).

The results for the test scenarios with one and two extended sources (shown in the first row of Fig. 3) are presented in Table 1. Note that the results are in accordance with the qualitative comparisons displayed in Fig. 3: the proposed parametric image reconstruction method is by far superior to the EM and the MAP algorithms.

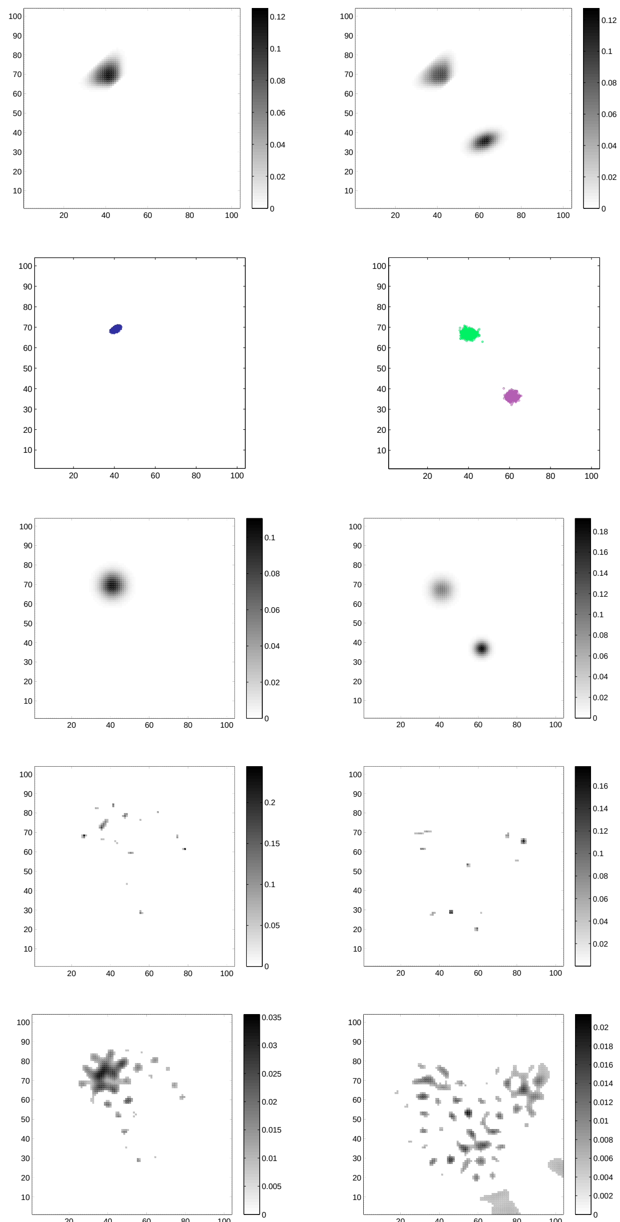

Fig. 3. Single run simulation results for one (left column) and two (right column) extended sources. First row: the original images; Second row: the final PC source-location samples; Third row: reconstructed images using the proposed algorithm; Forth row: reconstructed images using the EM method; Fifth row: reconstructed images using the MAP method with the Gibbs prior

Table 1. Image reconstruction error $\mathcal{E}$, averaged over 100 Monte Carlo runs (standard deviations in brackets)

	Single source	Two sources
Proposed	5.35 (1.08)	16.29 (4.11)
EM	20.61 (2.12)	34.69 (1.38)
MAP	17.92 (1.35)	32.79 (1.08)

5. CONCLUSIONS

The paper considered the problem of image reconstruction for an RMC gamma-ray imaging device, prototyped by DSTO. This instrument was developed for the purpose of localisation of radiological sources within its field of view. Since the expected number of such sources is relatively small, and their extent can be approximated by shapes in a parametric form (e.g. circle, ellipse), the paper proposed a parametric Bayesian image reconstruction algorithm. The advantage of this approach is a dimension reduction. Preliminary results show improved performance for extended sources, in comparison with the standard algorithms used in emission tomography for medical imaging. In its current form, the proposed algorithm requires one to specify the number of sources Q. Future work will incorporate a model selection logic [12] for a joint estimation of Q and the parameter vector $\boldsymbol{\theta}$.

6. REFERENCES

[1] C. D. Ferguson, K. Tahseen, and J. Birira, "Commercial radioactive sources: surveying the security risks," Monterey Institute of International Studies, Center for Nonproliferation Studies, 2003.

[2] M. Roberts, A. Eleftherakis, and M. Kocan, "The development of prototype gamma ray imagers for radiological source search," in *Proc. Future Land Force Conf.* Brisbane, Australia, Sep. 2014.

[3] B. R. Kowash, D. K. Wehe, and J. A. Fessler, "A rotating modulation imager for locating mid-range point sources," *Nuclear Instruments and Methods in Physics Research A*, vol. 602, pp. 477–483, 2009.

[4] M. Defrise, P. E. Kinahan, and C. J. Michel, "Image reconstruction algorithms in PET," in *Positron Emission Tomography*, D. L. Bailey, D. W. Townsend, P. E. Valk, and M. N. Maisey, Eds., chapter 4. Springer, 2003.

[5] L. A. Shepp and Y. Vardi, "Maximum likelihood reconstruction for emission tomography," *IEEE Trans Medical Imaging*, vol. 1, no. 2, pp. 113–122, 1982.

[6] K. Lange, "Convergence of EM image reconstruction algorithms with Gibbs smoothing," *IEEE Trans. Medical Imaging*, vol. 9, no. 4, pp. 439–446, 1990.

[7] R. M. Leahy and J. Qi, "Statistical approaches in quantitative positron emission tomography," *Statistics and Computing*, vol. 10, pp. 147–165, 2000.

[8] J. Ma, Q. Feng, Y. Feng, J. Huang, and W. Chen, "Generalized Gibbs priors based positron emission tomography," *Computers in Biology and Medicine*, vol. 40, pp. 565–571, 2010.

[9] C. Musso, N. Oudjane, and F. LeGland, "Improving regularised particle filters," in *Sequential Monte Carlo methods in Practice*, A. Doucet, N. de Freitas, and N. J. Gordon, Eds., chapter 12. Springer-Verlag, New York, 2001.

[10] M. D. Martin, *Radial basis functions: Theory and Implementations*, Cambridge University Press, 2003.

[11] Y. Boers, E. Sviestins, and H. Driessen, "Mixed labelling in multitarget particle filtering," *IEEE Trans Aerospace and Electronic Systems*, vol. 46, no. 2, pp. 792–802, 2010.

[12] E. Makalic, D. F. Schmidt, and A. K. Seghouane, "A tutorial on model selection," in *Signal processing theory and machine learning*, R. Chellappa and S. Theodoridis, Eds., vol. 1 of *Academic press library in signal processing*, chapter 25, pp. 1415–1452. Elsevier, Oxford, UK, 2014.